Human Molecular Genetics, 2015, Vol. 24, No. 3 **727–739**
doi:10.1093/hmg/ddu491
Advance Access published on September 26, 2014

Sacs knockout mice present pathophysiological defects underlying autosomal recessive spastic ataxia of Charlevoix-Saguenay

Roxanne Larivière[1], Rébecca Gaudet[1], Benoit J. Gentil[2], Martine Girard[2], Talita Cristiane Conte[1], Sandra Minotti[2], Kim Leclerc-Desaulniers[1], Kalle Gehring[3], R. Anne McKinney[4], Eric A. Shoubridge[2], Peter S. McPherson[2], Heather D. Durham[2] and Bernard Brais[1,*]

[1]Department of Neurology and Neurosurgery, Laboratory of Neurogenetics of Motion and [2]Department of Neurology and Neurosurgery, Montreal Neurological Institute, McGill University, Montreal, QC, Canada H3A 2B4, [3]Groupe de Recherche Axé sur la Structure des Protéines, Department of Biochemistry and [4]Department of Pharmacology, McGill University, Montreal, QC, Canada H3G 0B1

Received August 2, 2014; Revised and Accepted September 22, 2014

Autosomal recessive spastic ataxia of Charlevoix-Saguenay (ARSACS [MIM 270550]) is an early-onset neurodegenerative disorder caused by mutations in the *SACS* gene. Over 170 *SACS* mutations have been reported worldwide and are thought to cause loss of function of sacsin, a poorly characterized and massive 520 kDa protein. To establish an animal model and to examine the pathophysiological basis of ARSACS, we generated *Sacs* knockout (*Sacs*$^{-/-}$) mice. Null animals displayed an abnormal gait with progressive motor, cerebellar and peripheral nerve dysfunctions highly reminiscent of ARSACS. These clinical features were accompanied by an early onset, progressive loss of cerebellar Purkinje cells followed by spinal motor neuron loss and peripheral neuropathy. Importantly, loss of sacsin function resulted in abnormal accumulation of non-phosphorylated neurofilament (NF) bundles in the somatodendritic regions of vulnerable neuronal populations, a phenotype also observed in an ARSACS brain. Moreover, motor neurons cultured from *Sacs*$^{-/-}$ embryos exhibited a similar NF rearrangement with significant reduction in mitochondrial motility and elongated mitochondria. The data points to alterations in the NF cytoskeleton and defects in mitochondrial dynamics as the underlying pathophysiological basis of ARSACS.

INTRODUCTION

Autosomal recessive spastic ataxia of Charlevoix-Saguenay (ARSACS [MIM 270550]) was first described in the French-Canadian population in 1978 (1). Since then, ARSACS cases have been reported worldwide (2). The ARSACS clinical phenotype consists of a childhood onset progressive spastic ataxia accompanied by sensory-motor polyneuropathy and thickening of the retina. People with ARSACS typically have abnormally increased muscle tone (spasticity), difficulty coordinating movements (ataxia), distal muscle wasting (amyotrophy), involuntary eye movements (nystagmus) and speech difficulties (dysarthria) (3,4). French-Canadian ARSACS patients, who often share the same homozygous c.8844 delT genotype, become wheelchair-bound, on average, by the age of 41 and life expectancy is reduced (5). Postmortem examination of ARSACS' brains has revealed atrophy of the anterior cerebellar vermis associated with Purkinje cell death, while the cerebellar hemispheres are less affected (6–8). Brainstem corticospinal tracts are small and there is a bilateral loss of myelin in both spinal cord corticospinal and posterior spinocerebellar tracts. Over 170 mutations in the human *SACS* gene have been identified (https://grenada.lumc.nl/LOVD2/mendelian_genes/home.php?select_db=SACS). This has broadened the clinical spectrum to cases ranging from a severe spastic paraparesis with important cognitive impairment to much milder forms presenting exclusively axonal peripheral

*To whom correspondence should be addressed at: Montreal Neurological Institute, Room 622, 3801, University Street, Montreal, QC, Canada H3A 2B4. Email: bernard.brais@mcgill.ca

neuropathy (9,10). There is no available therapy for ARSACS and treatment is largely symptomatic.

The *SACS* gene encodes the massive 520 kDa protein sacsin. This multidomain protein contains an ubiquitin-like domain at the N-terminus that binds to the proteasome (11), three large sacsin repeat regions suggested to have an Hsp90-like chaperone function (12,13), an XPCB C-terminal domain that binds to the Ube3A ubiquitin protein ligase (14), a DnaJ domain that binds Hsc70 (11,12), and a nucleotide-binding domain at the C-terminus that mediates sacsin dimerization (15). The nature of these domains suggest a role for sacsin in protein quality control (12). Sacsin has been localized to mitochondria in SH-SY5Y cells and in cultured rat hippocampal neurons, and loss of sacsin function in ARSACS fibroblasts results in a hyperfused mitochondrial network (11,16). However, the relationship between the potential chaperone function of sacsin and its role in mitochondrial morphology remains unknown.

To study the role of sacsin in a physiological context, *Sacs*$^{-/-}$ mice were generated and characterized. Behavioral analyses conducted over a 1 year period demonstrated that *Sacs*$^{-/-}$ mice have motor defects attributable in part to cerebellar dysfunction. The behavioral phenotype was accompanied by early and progressive Purkinje cell loss followed by motor neuron loss and muscle atrophy. Importantly, the absence of sacsin led to abnormal neurofilament (NF) accumulations in the somatodendritic region of various neuronal populations of sacsin null mice and in ARSACS brain. Immunolabelings and western blots demonstrate that these NFH accumulations are filled with the non-phosphorylated form of NFH (npNFH). Moreover, reduced mitochondrial motility and abnormal mitochondrial morphology developed in motor neurons cultured from *Sacs*$^{-/-}$ mice. Together, our results indicate that the *Sacs*$^{-/-}$ mouse is a well-suited rodent model of the human condition and suggest that disruption of mitochondria organization and positioning through alterations in cytoskeletal proteins cause ARSACS pathology.

RESULTS

Ataxia, motor deficit and muscle weakness in *Sacs*$^{-/-}$ mice

Sacs$^{-/-}$ mice are born in a Mendelian ratio, are indistinguishable from heterozygous and control littermates at birth, breed normally and can have a normal life span with many animals surviving more than 2 years. Nonetheless, between 7 and 10 months, *Sacs*$^{-/-}$ mice display a grossly abnormal gait mostly visualized by the lateral spreading of their rear paws. By 15 months, *Sacs*$^{-/-}$ mice display tremor and the gait abnormalities become more pronounced (see Supplementary material, Video S1).

To assess the ataxic phenotype in detail, we subjected the *Sacs*$^{-/-}$ mice to tests measuring balance, motor coordination and muscle strength (Fig. 1). Significant differences were observed between *Sacs*$^{-/-}$ and *Sacs*$^{+/+}$ (control) animals on the balance beam test as early as 40 days of age, when sacsin null animals took significantly more time to cross the beam and displayed a greater number of foot slips (Fig. 1A–D; Supplementary Material, Video S2). Results are presented according to sex since we observed the usual differences in performance between males and females in mice. Though *Sacs*$^{+/-}$ mice did not show a grossly abnormal gait, they did have a significant but smaller increase in crossing latencies and foot slips on the beam test (Fig. 1A–H). General motor coordination was assessed using the rotorod test (Fig. 1M–P). *Sacs*$^{-/-}$ mice showed significantly inferior performance compared with controls, with the most significant differences occurring at 90 days (Fig. 1M and N; Supplementary Material, Video S3). *Sacs*$^{+/-}$ females, unlike *Sacs*$^{+/-}$ males, also showed significant decreased rotorod performance compared with controls (Fig. 1M).

Considering that the sensory-motor neuropathy observed in ARSACS contributes to the patient's progressive weakness, we directly assessed muscle strength in the mice using the inverted grid test (Fig. 1Q). Starting at 120 days of age, female *Sacs*$^{-/-}$ mice displayed a significant and progressive decrease in muscle strength compared with aged-matched controls. Performance of *Sacs*$^{+/-}$ mice was between that of *Sacs*$^{-/-}$ and *Sacs*$^{+/+}$, but this difference was not statistically significant. Furthermore, when held by the tail, 365-day-old *Sacs*$^{-/-}$ mice exhibited hindlimb clasping behavior, a characteristic response indicative of neurological dysfunction of motor control pathways (Fig. 1R and S). Taken together, these results demonstrate that *Sacs*$^{-/-}$ have an early progressive balance deficit associated with declining motor performance and muscle weakness, all features shared with ARSACS patients.

Purkinje cell loss and axonal swellings in *Sacs*$^{-/-}$ mice

ARSACS patients display progressive degeneration of cerebellar Purkinje cells (6). *Sacs*$^{-/-}$ mice also presented progressive Purkinje cell loss by 90 days of age (Fig. 2D). Moreover, this Purkinje cell loss was restricted to the anterior medial part of the cerebellum, mimicking the pathology in ARSACS patients (Fig. 2A–E) (6). Purkinje cell loss in *Sacs*$^{-/-}$ mice was not restricted to the vermis but extended to the cerebellar hemispheres, namely the simple lobule and the medial part of the ansiform crus 1 lobule without affecting the paraflocculars lobes (Fig. 2C). Interestingly, axons of Purkinje cells from *Sacs*$^{-/-}$ mice had numerous swellings, also called torpedoes, characteristic of axonal degeneration (17–19). These swellings were observed as early as 30 days of age, prior to detectable neuronal loss (Fig. 2F–I). The number of axonal swellings significantly increased with time, with an average of 18 swellings per section in 30-day-old animals compared with 80 swellings at 90 days (Fig. 2J). Swellings were more prominent in axons arising from the anterior versus posterior cerebellar lobules of *Sacs*$^{-/-}$ mice (Fig. 2J). Together, these results demonstrate that *Sacs*$^{-/-}$ mice display a pattern of differential Purkinje cell loss similar to that observed in ARSACS patients, and indicate that axonal damage precedes loss of cell bodies.

Neuronal dysfunction without axonal loss in the corticospinal tract of *Sacs*$^{-/-}$ mice

ARSACS is characterized by progressive spasticity caused by loss of upper motor neurons. To determine if *Sacs*$^{-/-}$ mice present a similar pyramidal pathology, we carried out histological analysis of the dorsal corticospinal tract at the T12 level. No gross morphological changes or significant axonal loss were observed in *Sacs*$^{-/-}$ mice at 2 years of age (Fig. 3B–D). However, NeuroSilver staining, which labels intracellular

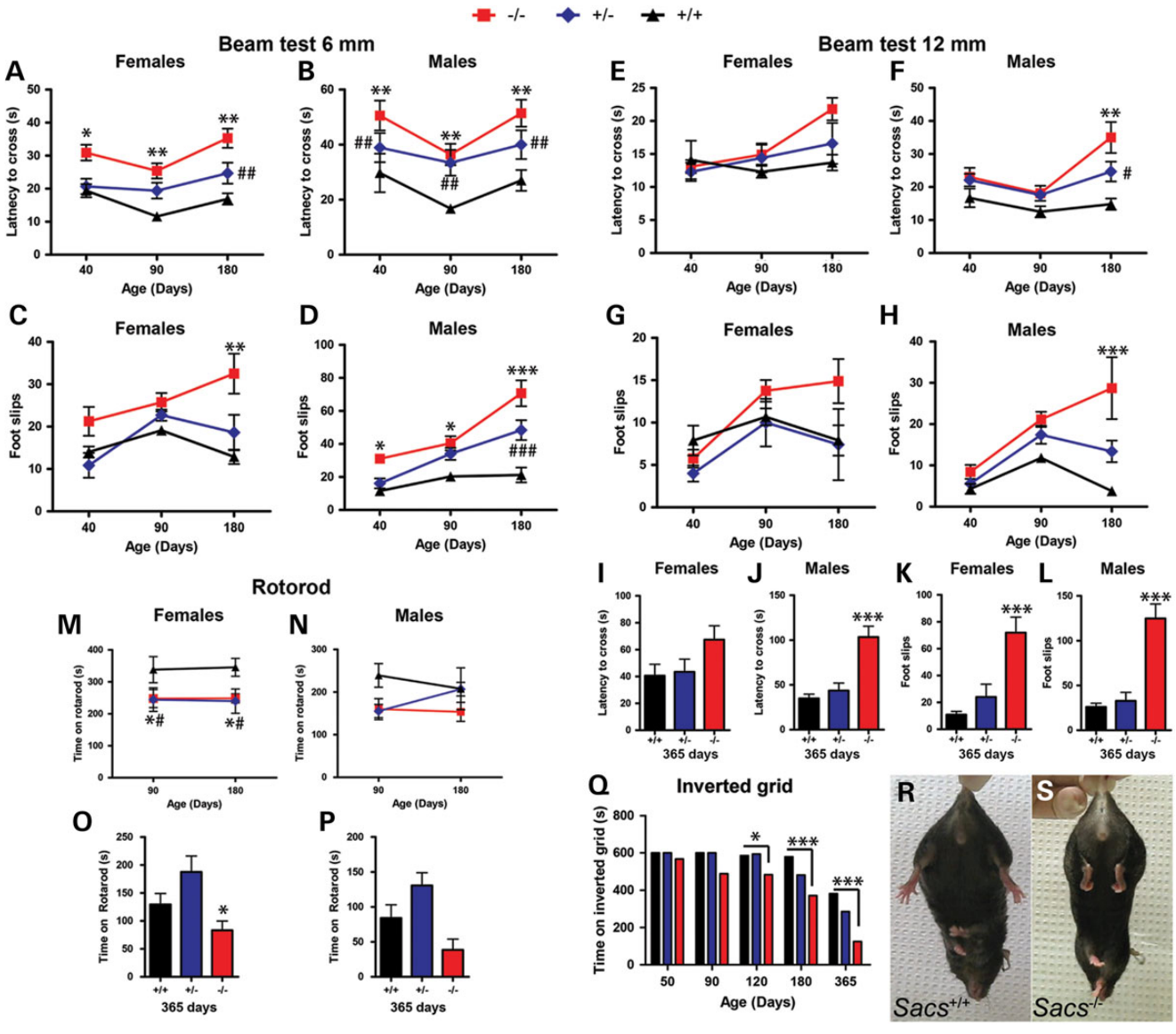

Figure 1. *Sacs*$^{-/-}$ mice display ataxia, motor deficit and muscle weakness. (**A–P**) Results of balance beam and rotorod tests of motor coordination for a first cohort of mice tested at 40, 90 and 180 days of age (A–D), (E–F), (M) and (N) and a second cohort tested at 365 days of age (I–L), (O) and (P). Deficits in both male and female mice as early as 40 days of age on the 6 mm beam test depicted by (A and B) increased latencies in crossing the beam and (C and D) increased number of foot slips. Heterozygous males also showed significant deficits compared with controls (A and D). (E–L) On the 12 mm beam, significant deficits were measured starting at 180 days for male (F), (H), (J) and (L) and at 365 days for female (K) *Sacs*$^{-/-}$ mice. (M and P) Significant motor deficit in *Sacs*$^{-/-}$ and *Sacs*$^{+/-}$ females compared with control mice on the accelerating rotorod test performed at 90, 180 (M and N) and 365 (O and P) days of age (M and O). Rotorod performance of *Sacs*$^{-/-}$ males was not significantly different from controls (N and P). (**Q**) Inverted grid test of mice at 50–365 days; significant muscle weakness in *Sacs*$^{-/-}$ females starting at 120 days of age compared with control mice. The difference between heterozygous mice and control was not statistically significant ($P > 0.05$). One-year-old *Sacs*$^{-/-}$ mice exhibited a hindlimb clasping reflex (**S**) rather than the normal plantar reaction (**R**). Data are presented as means ± SEM of three independent trials ($n \geq 7$ females and $n \geq 6$ males per group). $-/-$ versus $+/+$: $^{*}P < 0.05$, $^{**}P < 0.01$, $^{***}P < 0.005$; $+/-$ versus $+/+$: $^{\#}P < 0.05$, $^{\#\#}P < 0.01$, $^{\#\#\#}P < 0.005$ (two-way ANOVA with repeated-measures followed by Tukey's *post hoc* comparison of $-/-$ or $+/-$ versus $+/+$).

components in neurons undergoing degeneration, revealed prominent argyrophilic components with a 5.9-fold increase in intensity staining (Fig. 3E) in the *Sacs*$^{-/-}$ corticospinal tracts (arrow in Fig. 3I and M) compared with aged-matched controls (Fig. 3G and K). Similar silver-stained structures have been observed in somata, axons and terminals in both brain and spinal cord of animal models of other neurodegenerative disorders, such as spinocerebellar ataxia type 1, amyotrophic lateral sclerosis (ALS) and Alzheimer's and Huntington's diseases (20,21).

Peripheral neuropathy in *Sacs*$^{-/-}$ mice

The third major pathological feature of ARSACS is an evolving axonal sensory and motor polyneuropathy that contributes to both the ataxia and the progressive limb weakness (1). Since *Sacs*$^{-/-}$ mice develop distal weakness (Fig. 1Q), tissues were examined for anterior horn cell and peripheral nerve pathology (Fig. 4). At 2 years of age, counts of spinal motor neurons at the L5 level were reduced 25% in *Sacs*$^{-/-}$ mice compared with controls (Fig. 4C). In contrast, no obvious axonal degeneration

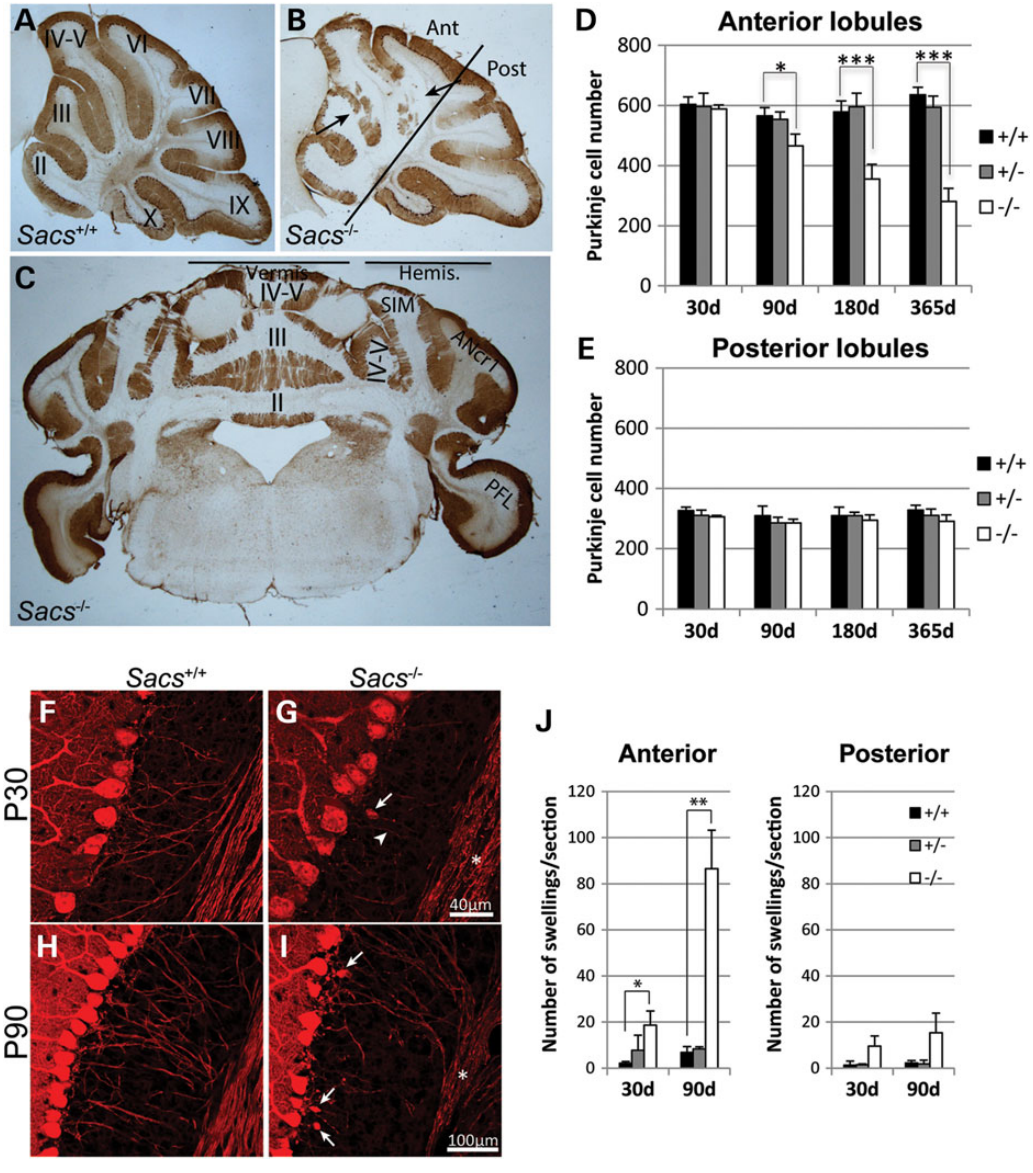

Figure 2. Progressive Purkinje cell loss and axonal swellings in *Sacs*$^{-/-}$ are restricted to the anterior lobules. (**A**–**C**) Anti-calbindin D-28K immunohistochemistry on mid-sagittal brain sections from 365-day-old *Sacs*$^{+/+}$ (A) and *Sacs*$^{-/-}$ (B) mice revealed Purkinje cell loss in the cerebellar anterior lobules, II to V of *Sacs*$^{-/-}$ mice (arrows). On coronal sections of *Sacs*$^{-/-}$ brain, Purkinje cell loss was restricted to the vermis and the medial hemispheres, namely the simple (SIM) and ansiform crus 1 (ANcr1) lobules, with sparing of the paraflocular lobe (PFL in C). (**D** and **E**) Neuronal cell counts in the anterior (I to VI) and posterior (VII to X) lobules at different ages, showing significant loss of Purkinje cells in *Sacs*$^{-/-}$ mice starting at 90 days of age in the anterior lobules (D), but not in the posterior lobules (E). Data represent means ± SD, $n = 4–5$ mice per group. (**F**–**I**) Anti-calbindin D-28K labeling of cerebellar parasagittal brain sections of 30-day-old *Sacs*$^{-/-}$ mice revealing dystrophic axons (asterisk and arrowhead in G) and occasional torpedo swellings in the proximal axonal segment (arrow in G) compared with *Sacs*$^{+/+}$ mice (F) (scale bar = 40 μm). (I) Numerous axonal swellings (arrows) and beaded axons (asterisk) were present in *Sacs*$^{-/-}$ samples at 90 days of age compared with age-matched controls (H) (scale bar = 100 μm). (J) Significant increase in numbers of axonal swellings in the cerebellar anterior lobules of *Sacs*$^{-/-}$ mice. Data represent means ± SD, $n =$ 3 mice per group; $^{*}P < 0.05$, $^{**}P < 0.01$, $^{***}P < 0.001$ (unpaired *t*-test).

or myelin defect was detected in mid-thigh segments of sciatic nerves (Fig. 4D and E). However, upon examination of axonal caliber distribution, *Sacs*$^{-/-}$ mice displayed a significant decrease in the number of large myelinated axons (7–10 μm diameter) (Fig. 4F), and a significant increase in the relative number of axons of diameter of 3–4 μm (Fig. 4F). Calf muscles of 2-year-old *Sacs*$^{-/-}$ animals showed significant loss in weight of gastrocnemius muscle (Fig. 4G and J) and to a lesser degree, the soleus (Fig. 4K). On H&E-stained sections of gastrocnemius muscle from *Sacs*$^{-/-}$ mice, some angular atrophic muscle fibers were present as well as hypertrophic fibers that could suggest some degree of neurogenic muscle atrophy (arrows in Fig. 4I). Thus, *Sacs*$^{-/-}$ mice manifest the three major features observed in ARSACS patients: cerebellar ataxia with Purkinje neuronal loss, upper motor neuron axonopathy and peripheral neuropathy.

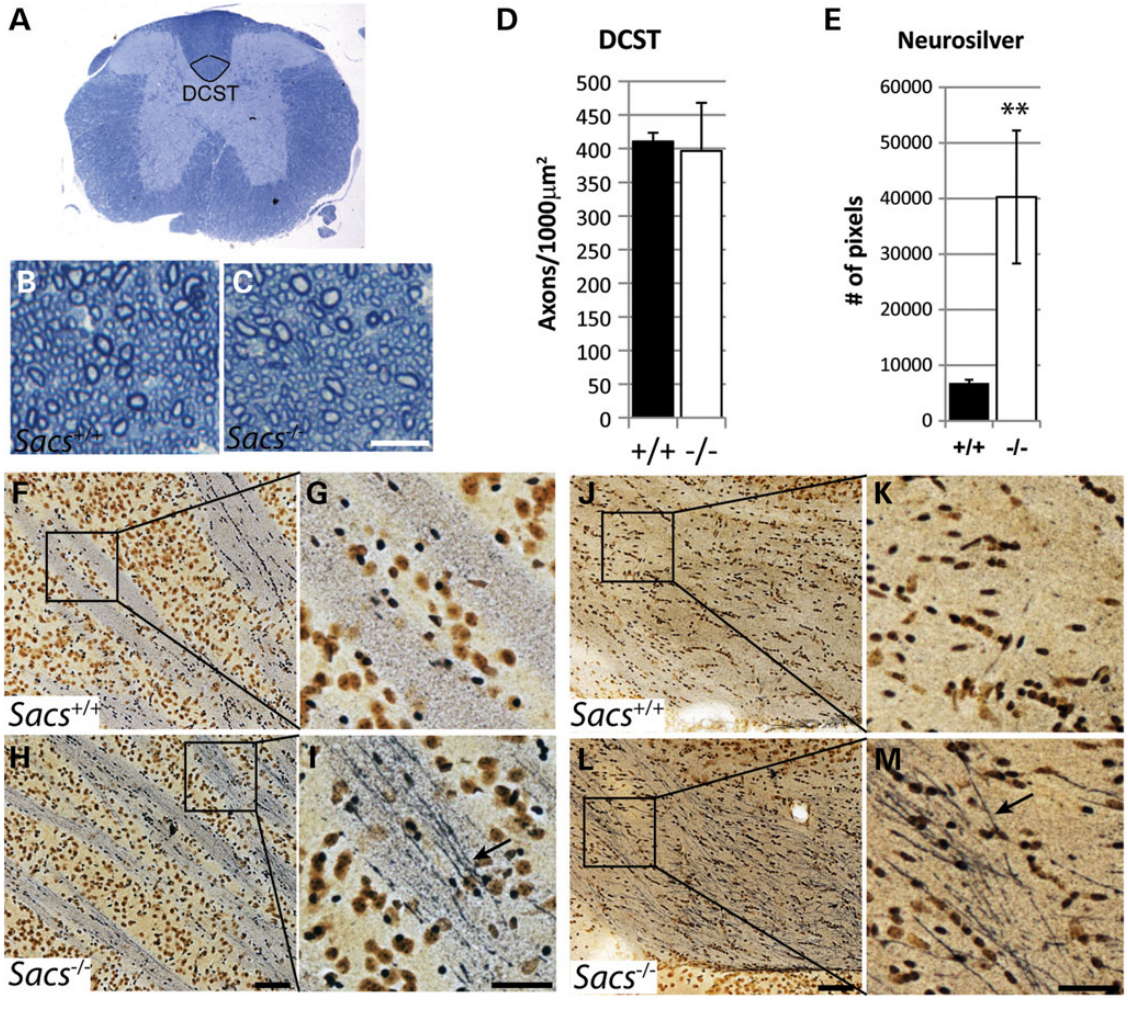

Figure 3. The number of corticospinal axons in *Sacs*$^{-/-}$ mice does not change significantly, but axons show signs of degeneration. (**A**) Low power cross section of the thoracic spinal cord of a *Sacs*$^{+/+}$ mouse at T12 level with the dorsal corticospinal tract (DCST) outlined. (**B** and **C**) Higher power images of toluidine-blue stained 1 μm semi-thin sections from 2-year-old *Sacs*$^{-/-}$ (C) and age-matched *Sacs*$^{+/+}$ (B) mice showing a portion of the DCST (Scale bar = 10 μm). No difference in gross morphology (B and C) or significant loss of corticospinal axons (**D**) was detected. Data presented are means ± SD of counts from three mice per group. (**E**–**M**) Neurosilver stain of parasagittal brain sections of *Sacs*$^{-/-}$ and *Sacs*$^{+/+}$ mice. Quantification of Neurosilver stain pixels show a 5.9-fold increase in cerebral peduncle of Sacs$^{-/-}$ mice compared with controls (E). Greater silver impregnation in corticospinal axons within the internal capsule (arrow in I) and cerebral peduncle (arrow in M) of *Sacs*$^{-/-}$ compared with age-matched *Sacs*$^{+/+}$ mice (G and K). Arrows point to argyrophilic components within *Sacs*$^{-/-}$ axons (scale bar = 100 μm in H and L and 50 μm in I and M). Data represent means ± SD, $n = 3$ mice per group; $^{**}P < 0.01$ (unpaired *t*-test).

NF accumulations in *Sacs*$^{-/-}$ and ARSACS brains

In examining cerebellar development in postnatal Day 7 (P7) and P14 *Sacs*$^{-/-}$ mice pups, no defects in lobulation or Purkinje cell migration were detected (Fig. 5A–D). However, a slight increase in NFs was detected in proximal dendrites in P14 *Sacs*$^{-/-}$ pups by labeling with pan-NFH antibody (Fig. 5F). NFs are neuronal intermediate filaments, that are composed of three major NF subunits in mature neurons, light (NFL), medium (NFM) and heavy (NFH) molecular-weight subunits (22,23). The pattern of NFH-labeling was distinctive from control in numerous brain regions of adult *Sacs*$^{-/-}$ mice. Somatodendritic NF accumulations were most striking in thalamic neurons, Purkinje cells and neurons in deep cerebellar nuclei, and the superior olive, but this phenotype was never present in controls (Fig. 6) (for a complete list of brain regions exhibiting somatodendritic NF accumulations refer to Supplementary Material, Table S1). Importantly, we observed the same pattern of NFH distribution in layer 5 cortical neurons and in Purkinje cells in an ARSACS brain, which further strengthens the resemblance between this mouse model and ARSACS (Fig. 6E and J). Immunolabeling using NFH phospho-dependent antibodies revealed that cell bodies and dendrites of Purkinje cells in *Sacs*$^{-/-}$ mice are intensely stained with the npNFH antibody (SMI32), whereas there is no difference in labeling with the phospho-NFH antibody (SMI31) compared with controls (Fig. 7A–D). Western blot analyses using pan-NFH antibody (N52) and phospho-dependent antibodies (SMI31, SMI32) further confirmed that the ratio of npNFH over NFH total protein levels is significantly increased by 24% in *Sacs*$^{-/-}$ mice compared with controls, whereas the level of pNFH as well as the levels of other NF proteins were unchanged (Fig. 7E and F). We observed the same significant increase in npNFH in cortex, spinal cord and sciatic nerves tissues of

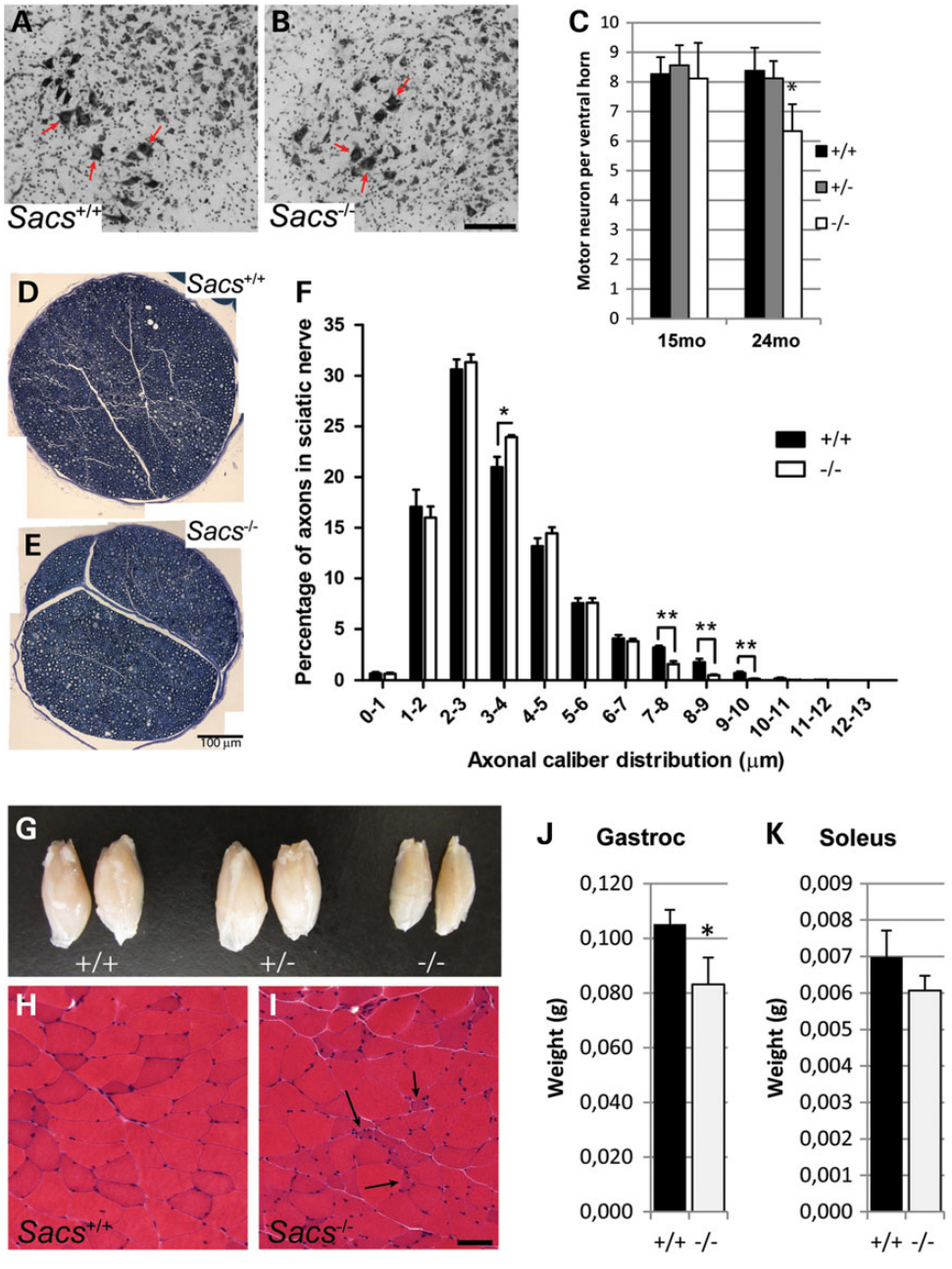

Figure 4. *Sacs*$^{-/-}$ mice develop a peripheral neuropathy. (**A** and **B**) Nissl-stained spinal cord cross-sections showing large motor neurons (arrows) in *Sacs*$^{+/+}$ (A) and *Sacs*$^{-/-}$ (B) mice (scale bar = 100 µm). (**C**) Motor neuron counts from 15- and 24-month-old *Sacs*$^{-/-}$, +/− and +/+ animals showing a 25% decrease at 24 months in *Sacs*$^{-/-}$ mice. Data presented as means ± SD, $n = 3$ mice per group; * $P < 0.05$ (unpaired *t*-test). (**D** and **E**) Toluidine-blue stained 1 µm semi-thin sections of sciatic nerves from 2-year-old *Sacs*$^{-/-}$ (E) and *Sacs*$^{+/+}$ (D) mice (scale bar = 100 µm). (**F**) Distribution of axonal calibers in sciatic nerve showing a shift in relative size distribution in *Sacs*$^{-/-}$ samples, with significant increase in the 3–4 µm range and decrease of large caliber axons (7–8, 8–9 and 9–10 µm). Data presented are means ± SEM of relative percentage of axons in each bin of diameters. $n = 5$ *Sacs*$^{-/-}$ and 4 *Sacs*$^{+/+}$ sciatic nerves; *$P < 0.05$, **$P < 0.01$ (unpaired *t*-test). (**G**) Decreased size of calf muscles from 2-year-old *Sacs*$^{-/-}$ mice. (**H–I**) H&E stained transverse sections of gastrocnemius muscle from 15-month-old animals showing angular atrophic muscle fibers in *Sacs*$^{-/-}$ muscle (arrows in I) (Scale bar in H = 50 µm). (**J** and **K**) Significant reduction in weight of gastrocnemius muscle (J), but not soleus muscle (K), from 2-year-old animals in *Sacs*$^{-/-}$ mice. Data presented are means ± SD, $n = 3$ mice per group; *$P < 0.05$ (unpaired *t*-test).

Sacs$^{-/-}$ mice (Supplementary Material, Fig. S2). Increases in npNFH were also detected in ARSACS brain biopsies taken from the motor cortex, hippocampus and cerebellum (Fig. 7G and H). Thus, the lack of sacsin perturbs the neuronal cytoskeletal network by specifically altering the level and organization of npNFH.

NF accumulations and defective axonal transport in *Sacs*$^{-/-}$ motor neurons

The effect of sacsin's absence on the cytoskeleton was further examined in motor neurons of dissociated spinal cord cultures [which include dorsal root ganglia (DRG)] prepared from

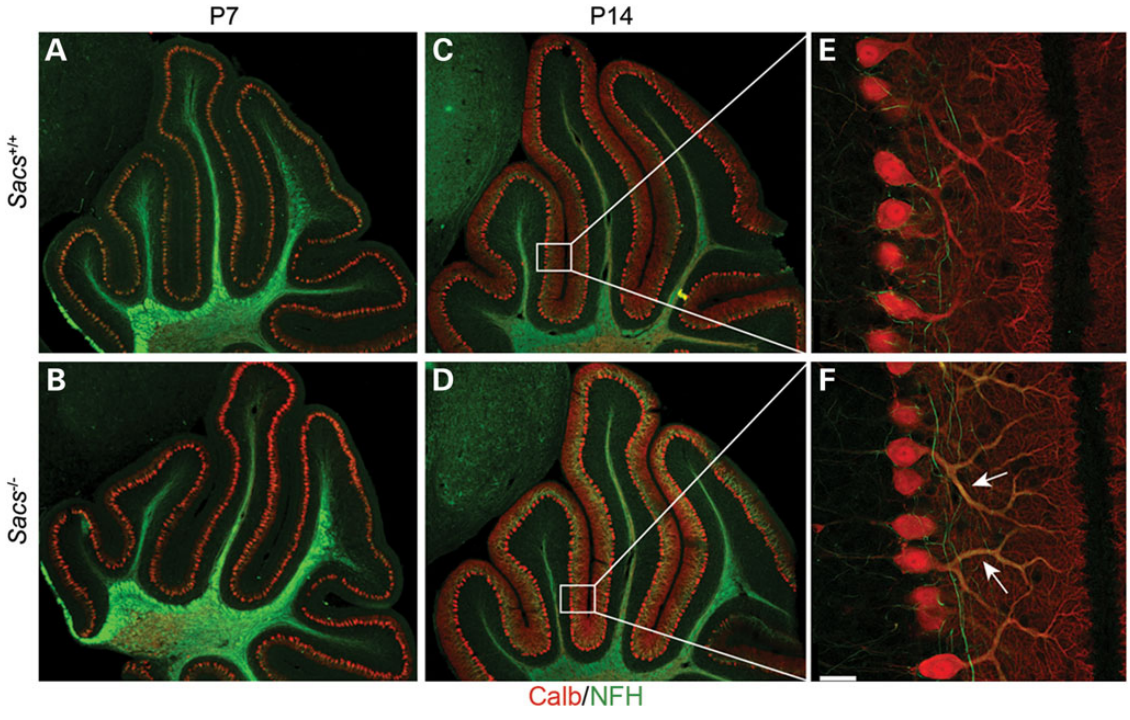

Figure 5. Cerebellar development is normal in *Sacs*$^{-/-}$ mice, but levels of NFH are increased in Purkinje dendrites. Double immunolabeling of sagittal sections of cerebella with anti-calbindin D-28K and anti-NFH antibodies at P7 (**A** and **B**) and P14 (**C**–**F**) demonstrates no defect in cerebellar lobulation and foliation in *Sacs*$^{-/-}$ animals (B and D), but shows increased level of NFH in Purkinje cell dendrites of *Sacs*$^{-/-}$ mice at P14 (F) compared with controls (E) (scale bar = 35 μm).

Sacs$^{-/-}$ embryos. A delay in maturation was observed in motor neurons in these cultures compared with *Sacs*$^{+/+}$ cultures. Absence of sacsin was associated with a delay of about 2 weeks in achieving maximal mean cell body diameter (≥20 μm) (Fig. 8A) and a sustained peripherin expression, a neuronal intermediate filament protein that normally decreases as motor neurons mature (Fig. 8B). At 21 and 42 days *in vitro* (DIV), *Sacs*$^{-/-}$ spinal cord motor neurons showed similar NF bundling and accumulation in the somatodendritic compartment as neurons *in vivo* (Fig. 8C–F). A similar redistribution of NF was observed in cultured hippocampal neurons in which sacsin was knocked down using lentiviral expression of shRNA targeting sacsin (Supplementary Material, Fig. S3).

Since NFs play a role in the regulation of mitochondrial morphology and motility (24), and mitochondrial abnormalities were observed in ARSACS fibroblasts and in cultured hippocampal cells following knockdown of sacsin (16), we next investigated the effect of sacsin knockout on mitochondrial transport in spinal cord motor neuron axons. At DIV21, mitochondrial motility was significantly reduced in axons of *Sacs*$^{-/-}$ motor neurons in which only 8% of mitochondria underwent unidirectional movement compared with 32% in axons of control cultures (Fig. 8G). At DIV35, the percentage of motile mitochondria in *Sacs*$^{-/-}$ axons had decreased to 3–4% compared with 20% in the controls (Fig. 8I). This significant decrease in motility was not associated with a change in the velocity of mitochondrial movements (Fig. 8H and J).

As previously reported in fibroblasts from ARSACS patients (16), axonal mitochondrial morphology was also affected in *Sacs*$^{-/-}$ motor neurons. Mitochondrial length was comparable with controls in motor neurons of *Sacs*$^{-/-}$ cultures at DIV21, but was drastically increased at DIV35 (Fig. 8K–L). Important to note is that NF bundling (Fig. 8D) and increase in mitochondrial stationary time (Fig. 8G) were evident by DIV21, prior to significant increase in mitochondrial length (Fig. 8M).

DISCUSSION

This study demonstrates that loss of sacsin function in *Sacs*$^{-/-}$ mice recapitulates well the major clinical and pathological features of ARSACS. *Sacs*$^{-/-}$ mice manifest a progressive gait defect associated with Purkinje cell loss, cortical motor neuron and pyramidal tract pathology and a polyneuropathy leading to distal muscle weakness. We did not observe a sex influence on the phenotype. Both male and female knockout mice had a similar phenotype visualized by performance values that followed the same trend over time. As in ARSACS patients, the first measurable motor deficit in *Sacs*$^{-/-}$ mice is reported at 40 days and is associated with abnormal balance shown by the beam test performance. These gait difficulties precede extensive cerebellar neuronal loss, suggesting that the early ataxic gait phenotype reflects neuronal dysfunction and not neuronal death. Purkinje cells in *Sacs*$^{-/-}$ mice slowly and progressively degenerate, starting between 2 and 3 months of age and continuing beyond 1 year. As observed in ARSACS patients, the most affected Purkinje cells in *Sacs*$^{-/-}$ mice are localized to the anterior lobules in the rostral–caudal axis and in the vermis and paravermis in the medial–lateral axis. These Purkinje axons terminate in the fastigial and interposed cerebellar nuclei, which in turn project to both the cerebral cortex via the thalamus, and to brainstem nuclei, to modulate the descending pyramidal motor tracts that

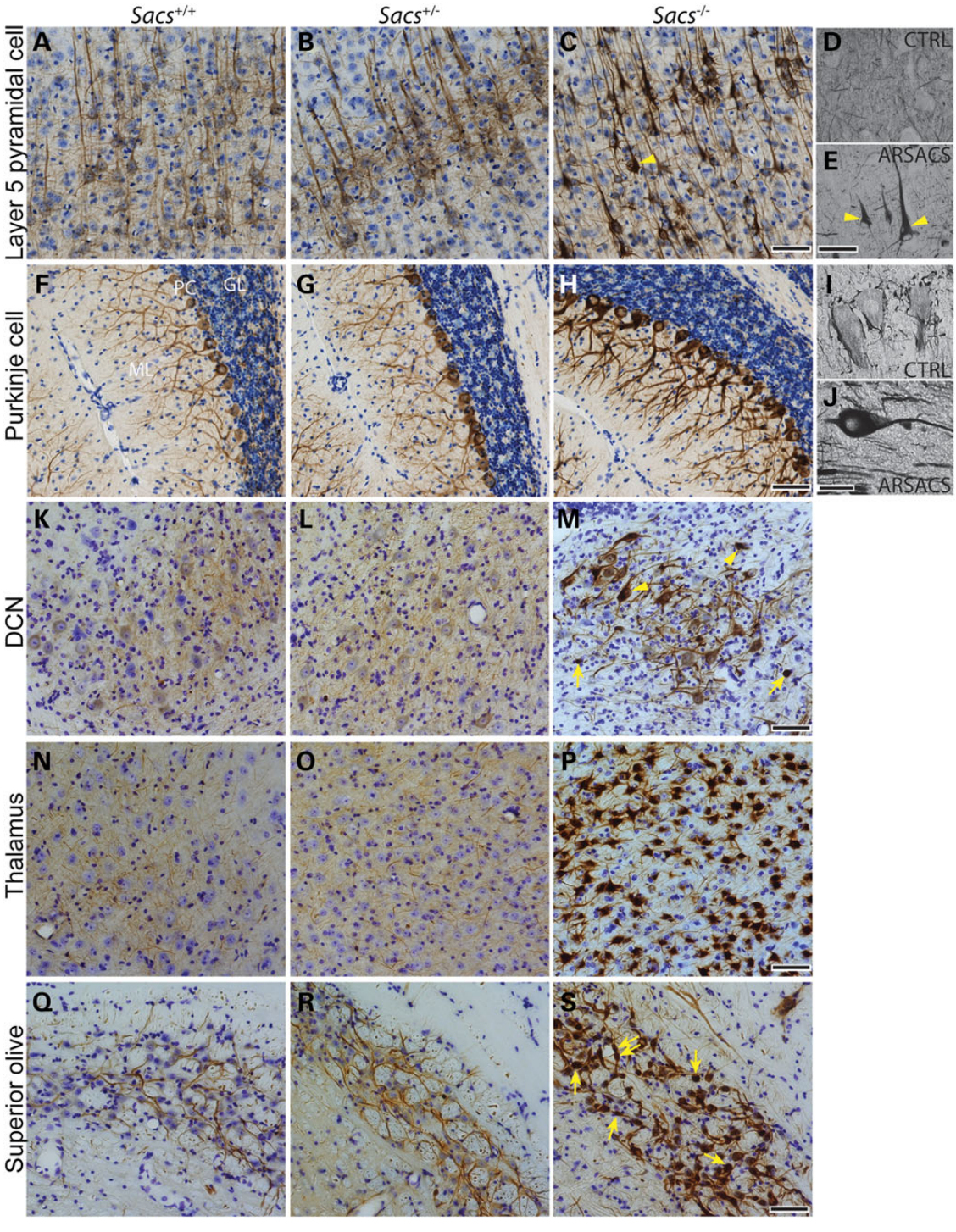

Figure 6. NF accumulations in *Sacs*$^{-/-}$ and ARSACS neurons. (**A**–**C**), (**F**–**H**) and (**K**–**S**) NFH immunohistochemistry on sagittal brain sections of 180-day-old mice and on brain sections from a human control autopsy case (**D** and **I**) and one ARSACS case (**E** and **J**). NF accumulations are present in *Sacs*$^{-/-}$ and ARSACS neuronal populations, such as layer 5 pyramidal cells (A–E), Purkinje cells (F–J), neurons of the deep cerebellar nuclei (DCN) (K–M), thalamic neurons (N–P) and superior olive neurons (**Q**–**S**). Nuclear displacement to the periphery is shown in pyramidal cells and neurons of deep cerebellar nuclei with NF accumulations (arrowheads in C, E and M). NF containing swellings are seen in neurons of deep cerebellar nuclei and superior olive (arrows in M and L) (scale bar = 100 μm in C, H, M, P and L and 50 μm in E and J).

regulate trunk and limb movements and that are important for normal gait. The dysfunction of these regulatory motor pathways could in part explain the cerebellar ataxia observed in *Sacs*$^{-/-}$ mice and patients. However, along with the degenerating PC, *Sacs*$^{-/-}$ mice show abnormal NFH accumulations in many CNS cell populations, which appear to follow the relative regional neuronal expression of sacsin (11). Among those, motor thalamic neurons are particularly affected and show massive NFH

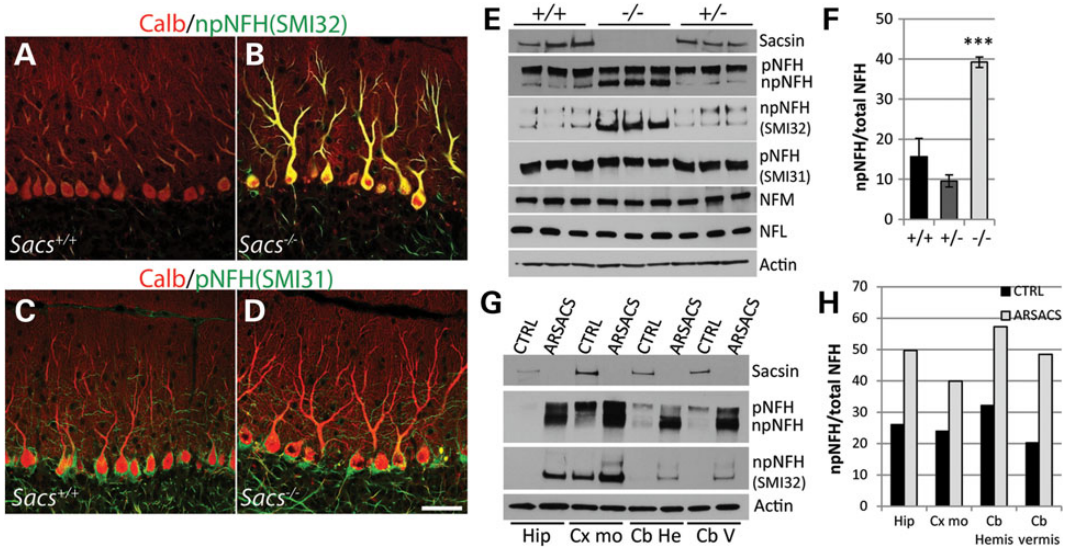

Figure 7. Non-phosphorylated NFH levels are significantly increased in *Sacs*$^{-/-}$ mice and ARSACS. (**A**–**D**) Double immunolabelings against calbindin D-28K and non-phosphorylated (npNFH in A and B) and phosphorylated (pNFH in C and D) NFH show intense npNFH labeling of PC somata and dendrites in *Sacs*$^{-/-}$ mice (B) compared with controls (A). No significant change in pNFH labeling is observed between *Sacs*$^{-/-}$ (D) and controls (C). (**E**) Immunoblots of cytoskeletal fractions extracted from cerebella of *Sacs*$^{+/+}$, +/− and −/− mice show increased levels of npNFH in *Sacs*$^{-/-}$ homogenates when probed with pan-NFH antibody as well as when probed with npNFH-specific antibody (SMI32). Levels of other NF proteins, NFL and NFM are unchanged (E). (**F**) The ratio of npNFH over total NFH levels is significantly increased by 24% in *Sacs*$^{-/-}$ mice compared with controls. (**G**) Western blot of cytoskeletal fractions extracted from ARSACS postmortem biopsies taken from the hippocampus (Hip), the motor cortex (Cx mo) and the cerebellar hemispheres (Cb He) and vermis (Cb V) also show increased levels of npNFH using a pan-NFH antibody and npNFH-specific antibody (SMI32). (**H**) As observed in *Sacs*$^{-/-}$ mice, the ratios of npNFH over total NFH levels are also increased in all ARSACS tissues. Data are presented as means ± SD. Data represent means ± SD, $n = 3$ mice per group; $^{*}P < 0.05$, $^{**}P < 0.01$, $^{***}P < 0.001$ (unpaired *t*-test) −/− versus +/+ (scale bar in D = 100 μm).

protein accumulation within their somatodendritic region (Fig. 6P). Given that the motor thalamus is an important relay center that integrates and modulates information incoming not only from the cerebellum and spinal cord somatosensory system but also from the basal ganglia to generate and modulate movement, it is highly possible that defects in thalamic circuitries influence greatly the observed phenotype in *Sacs*$^{-/-}$ mice and patients. Indeed, focal lesions of the thalamus have been associated with ataxia, dystonia, pyramidal weakness and many other motor symptoms, as well as numerous behavioral abnormalities (25–27). Two independent groups documented abnormal thalamic MRI signals in Italian and Turkish ARSACS patients, further suggesting that involvement of defective thalamic relays might be associated with the spastic ataxia phenotype in these patients (28,29). Moreover, observations of NFH accumulations intrinsic to cortical pyramidal neurons, increased silver impregnation in corticospinal axons, and loss of L5 motor neurons suggests that dysfunction of the corticospinal afferents most likely also contributes to the progressive motor impairment and might lead to the observed muscle weakness in *Sacs*$^{-/-}$ mice.

Disorganization of the NF network is the earliest cytopathological change identified in *Sacs*$^{-/-}$ neurons, a feature also identified in ARSACS brain. This study also reports an accumulation of npNFH, with unchanged levels of the other NF proteins, in *Sacs*$^{-/-}$ and ARSACS neuronal tissues. Whether these accumulations are a result of a disrupted turnover or aberrant posttranslational modifications remains unknown, but it is certainly uncommon in neurodegenerative disorders to exhibit increases in npNFH. Indeed, the NFH accumulations seen in *Sacs*$^{-/-}$ mice and ARSACS do not resemble injury-related changes in NFM/NFH, which are typically manifested by increased phosphorylation of NFM and NFH C-terminal KSP repeat domains (30–32). Nonetheless, NF disorganization has been observed in many neurological disorders such as ALS, Alzheimer's and Parkinson diseases, and is thought to be involved in the pathogenesis of these diseases (23,33,34). The presence of NF accumulations in the somatodendritic region of PC as early as P14, prior to neuronal loss, and the fact that we observe these NF accumulations in numerous neuronal populations in *Sacs*$^{-/-}$ mice, strongly suggests that alteration in the cytoskeletal network is a key early cellular dysfunction in ARSACS. Although no direct interaction between NFs and sacsin has been reported, sacsin has been found to interact with α-actinin-4 (35). The α-actinins belong to a family of actin-binding proteins that cross-link and bundle actin filaments (36) and are involved in the organization of the submembranous cortical cytoskeleton (37,38). Since it is well established that NFs are organized into an extensively cross-linked cytoskeletal network with microtubules and actin microfilaments through multiple cross-bridging proteins (39–41), it can be hypothesize that sacsin could be an important organizer of the cytoskeletal network. Axonal torpedos were identified in Purkinje cells in *Sacs*$^{-/-}$, and although not specific to either Purkinje neurons or ARSACS, they have been associated with an abnormal cytoskeleton and obstruction of axonal transport in other degenerative disorders such as ALS (23,33,34).

We previously reported accumulation of mitochondria in proximal dendrites of cultured hippocampal neurons after knockdown of sacsin and elongated mitochondria in fibroblasts cultured from an ARSACS affected individual (16). Here, we further explored the effect of loss of sacsin function on mitochondrial dynamics and the relationship with accumulations of

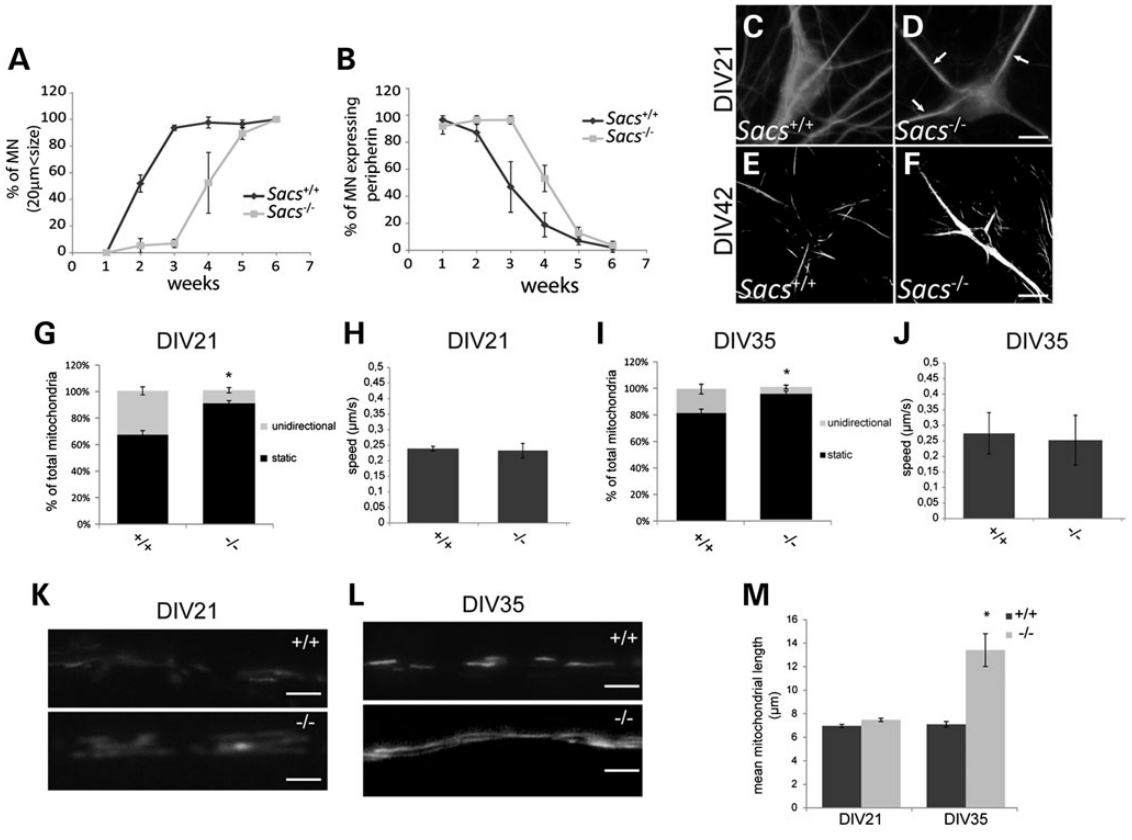

Figure 8. (**A**–**F**) Delayed maturation of cultured *Sacs*$^{-/-}$ spinal motor neurons. (A) Delay in the percentage of motor neurons having reached diameter ≥20 µm and (B) in loss of the developmentally regulated NF protein, peripherin, in dissociated spinal cord cultures from *Sacs*$^{-/-}$ embryos. (C–F) Anti-NFH immunolabeling of DIV21 (C and D) and DIV42 (E and F) cultures showing accumulation of NF bundles (arrows) in *Sacs*$^{-/-}$ motor neurons. (**G**–**M**) Defects in mitochondrial transport and morphology in cultured *Sacs*$^{-/-}$ motor neurons. The percentage of motile mitochondria (versus static) is decreased in motor neuron axons in *Sacs*$^{-/-}$ compared with *Sacs*$^{+/+}$ spinal cord cultures at DIV21 (G) and DIV35 (I). Average speed of mitochondrial movement (µm/s) was comparable in *Sacs*$^{-/-}$ and *Sacs*$^{+/+}$ motor neuron axons in DIV21 (H) and DIV35 (J) cultures (5–10 mitochondria per condition). (K–M) Increased mitochondrial length in DIV35 *Sacs*$^{-/-}$ cultures. Representative images of mitochondrially targeted dsRed in motor neuron axons in DIV21 (K) and DIV35 (L) *Sacs*$^{+/+}$ or *Sacs*$^{-/-}$ cultures. (M) Mean mitochondrial length ± SEM in motor neuron axons in 21 or 35 DIV *Sacs*$^{+/+}$ or *Sacs*$^{-/-}$ cultures. $n = 38–49$ mitochondria per condition; *Significantly different from *Sacs*$^{+/+}$, $P < 0.05$ (one-way ANOVA with Tukey HSD *post hoc* analysis).

NFs in motor neurons cultured from *Sacs*$^{-/-}$ mice. In these motor neurons, mitochondrial shape and frequency of movement was affected, but not the velocity of transport. The elongation of mitochondrial morphology occurred in older cultured *Sacs*$^{-/-}$ motor neurons (DIV35), subsequent to NF abnormalities. This raises the question whether abnormal NF homeostasis could lead to the mitochondrial phenotype observed in *Sacs*$^{-/-}$ neurons. Previous studies have linked NFs to the mitochondrial network (24,42,43). Indeed, NFH interacts with mitochondria *in vitro* and this interaction is affected by the phosphorylation state of NFH (43). Furthermore, Gentil *et al*. showed that SW13^{vim-} cells, which do not express any intermediate filament proteins endogenously, display elongated mitochondria when transfected with an NFL-encoding vector, arguing that interfering with proper intermediate filament composition directly modifies mitochondrial architecture (24). We thus propose that loss of sacsin function leads to altered NF organization and to altered cytoskeletal axonal architecture in a way that impairs mitochondrial localization and dynamics, making neurons particularly vulnerable to stress.

In conclusion, the *Sacs*$^{-/-}$ mouse recapitulates the major clinical and pathological features of ARSACS making it a well-suited rodent model, not only for therapeutic trials but also to study the function of sacsin and the consequences of its disruption on ARSACS.

MATERIALS AND METHODS

Behavioral tests

Mice were tested for balance, motor coordination and muscle strength using the balance beam, rotorod and inverted grid tests. For balance beam and rotorod testing, a first cohort was tested at 40, 90 and 180 days of age (females $n \geq 7$ per groups, males $n \geq 6$ per group) and a second cohort was tested at 365 days (females $n \geq 9$ per group, males $n \geq 7$ per group). For the inverted grid test, separate cohorts of 50, 90, 120, 180 and 365 days of age consisting of females only were tested ($n \geq 5$ per group). The balance beam test was performed as reported previously (44). For the rotorod test, mice were first trained on the apparatus at a constant speed of 4 rpm for five 10 min trials. After completion of training, animals were tested for three trials. Each mouse was placed on the apparatus, and the speed of rotation was gradually increased from 4 to 40 rpm. The latency until

the animal fell from the rotating rod was recorded, using a cutoff time of 5 min. For the inverted grid test, animals were tested for two trials with no previous training. Each mouse was put on the grid in a vertical position; the grid was then inverted upside down at a height of 25 cm above a padded cushion. The latency until the animal fell from the grid was recorded, using a cutoff time of 5 min.

Immunohistochemistry and NeuroSilver stain

For preparation of tissue sections, mice were anesthetized with mouse anesthetic cocktail [ketamine (100 mg/ml), xylazine (20 mg/ml) and acepromazine (10 mg/ml)], perfused transcardially with 0.9% NaCl followed by 4% paraformaldehyde. Brains were dissected and postfixed for 2 h at 4°C in the same fixative. Tissues were then equilibrated in 30% sucrose/PBS until sectioning. Sagittal sections (35 μm) were cut using a freezing sledge microtome. Free-floating sections were processed for immunohistochemistry. Sections were first processed for sodium citrate heated antigen retrieval followed by inactivation of endogenous peroxidase. Sections were then blocked in TBST (5% normal goat serum; 0.25% Triton X-100; 150 mM NaCl in 100 mM Tris, pH 7.4) and incubated with anti-calbindin-D-28K (Sigma, C2724, 1:1000) or anti-NFH antibody (Millipore, MAB5266, 1:2000) diluted in blocking buffer overnight at 4°C. Sections were then incubated with appropriate biotinylated secondary antibodies (Vectors Labs) followed by VECTASTAIN ABC reagent for 1 h, washed and reacted with VECTOR DAB substrate. Sections were mounted on Snowcoat X-tra slides (Surgipath), air dried, dehydrated in a graded series of ethanol dilutions, cleared in xylene, counterstained with cresyl-violet or not and coverslipped using Protocol mounting medium (Fisher Scientific). Imaging was performed using a Leica DMI6000 inverted microscope. For immunofluorescence detection, Alexa Fluor 555 conjugated goat anti-rabbit or Alexa Fluor 488 anti-mouse was used as secondary antibodies. Confocal imaging was performed using a Zeiss LSM 710 confocal microscope. NeuroSilver stain (FD Neurotechnologies, Inc.) was performed according to the manufacturer's protocol. To quantify Neurosilver stain, images were thresholded using constant parameters to capture argyophilic structures with ImageJ software. Thresholded pixels were then quantified using Adobe Photoshop CS6.

Muscle histology

Female mice were euthanized by CO_2 asphyxiation. Gastrocnemius and soleus muscles were dissected, weighed and frozen in liquid nitrogen-cooled isopentane. Six micrometers of transverse cryostat sections were prepared on glass slides. Unfixed sections were stained with hematoxylin and eosin (H&E) to reveal the general morphology and imaged using a Leica DMI6000 inverted microscope.

Purkinje cell and motor neuron counts

Purkinje cell counts were performed on 3–4 animals per group as previously described (16). For spinal motor neuron counts, 12–20 transverse spinal cord sections (35 μm) were mounted onto Snowcoat X-tra slides (Surgipath) and Nissl stained. Spinal motor neurons with cell bodies $\geq 600\ \mu m^2$ were counted by tracing neuronal cell bodies located in the spinal anterior horn using ImagePro Plus software (Media Cybernetics, Inc.).

Analysis of Purkinje cell axonal swellings

To count Purkinje cell axonal swellings, the first 10 vermal sections (25 μm) were labeled with anti-calbindin-D-28K and Alexa Fluor 555 conjugated goat anti-rabbit and mounted on Surgipath slides. The number of swellings in three transverse sections per animal (three animals per group) were counted starting from lobules I to VII inclusively, and then from VIII to X using a Zeiss Axio Observer microscope and ×40 objective.

Distribution of axon calibers

Mice were anesthetized as previously mentioned and perfused transcardially with 0.9% NaCl followed by 4% paraformaldehyde. Sciatic nerves were dissected and postfixed for 2 days at 4°C in 3% glutaraldehyde. A mid-thigh 2 mm portion of each sciatic nerve was postfixed in 2% osmium for 1 h at room temperature followed by dehydration and embedding in Epoxy resin 812. One micrometer of cross-sections were toluidine-stained and imaged using a Leica DMI6000 inverted microscope under a ×63 oil-immersion objective. The diameters of myelinated axons were measured using ImagePro Plus Software (Media Cybernetics, Inc.) and the distribution plotted in Excel software.

Western blots

Cytoskeletal (triton insoluble) fractions were prepared by homogenizing tissues with a Teflon putter in extraction buffer [10 mM Tris–HCl, pH 7.5, 150 mM NaCl, 1 mM 6 EDTA, 1% Triton X-100 and protease inhibitors (Roche)] followed by centrifugation at 12 000 *g* 15 min. Supernatant was removed and cytoskeletal proteins in the pellet were further homogenized in SUB buffer [0.5% SDS, 8 M urea, 2% β-mercarptoethanol]. Samples were centrifuged 20 min at maximum speed and supernatant (cytoskeletal fractions) was collected. Protein quantification was performed using the Bradford technique (Bio-Rad). Homogenates were separated onto a NuPAGE Tris Acetate gel (Life Technologies) and transferred onto a nitrocellulose membrane (Bio-Rad). Immunoblots were probed with rabbit polyclonal anti-sacsin, monoclonal anti-actin (clone C4, Millipore), anti-NFH (clone N52, Sigma-Aldrich), anti-pNFH (SMI31), anti-npNFH (SMI32) antibodies from Covance, anti-NFL (clone NR4, Abcam) and anti-NFM (clone NN18, Sigma-Aldrich).

Cytoskeletal and mitochondrial phenotypes in *Sacs*$^{-/-}$ cultured motor neurons

Cultures of dissociated spinal cord (also including DRG) were prepared from E13 embryos of *Sacs*$^{-/-}$ and *Sacs*$^{+/+}$ mice as previously described (45). Maturation of motor neurons *in vitro* was quantified by measuring cell body diameter and expression of the NF proteins, peripherin and NFH, at weekly intervals.

To measure mitochondrial shape and motility, plasmid encoding mitochondrial-targeted DsRed (pOCT-dsRed, 23 μg/ml)

was expressed in motor neurons by intranuclear microinjection (3 or 5 weeks after plating), as previously described (24). The identification of motor neurons was based on their characteristic morphology, previously validated using motor neuron markers (46). Coverslips were placed in a live cell imaging chamber (Harvard Apparatus) and mounted on the stage of a Zeiss observer Z1 inverted microscope equipped with epifluorescence optics. Images were captured using a $\times 63$ 1.4 NA Apochromat objective (Zeiss) and an ORCA-ER cooled CCD camera (Hamamatsu Photonics). The timelapse feature of Axiovision software (Zeiss) was set to acquire images of mitochondria in an axonal segment at 100 frames every 5 s (24). Photobleaching was minimal under those conditions. A mitochondrion was considered moving when change of position of at least 4 μm occurred on four consecutive frames (unidirectional movement). Unidirectional movement was recorded as anterograde or retrograde. Mitochondrial speed was estimated by the time for a mitochondrion undergoing unidirectional movement to cover 11 μm. Mitochondrial length was measured using Axiovision software.

Statistical analysis

Data for the behavioral phenotyping are presented as mean ± SEM. Data from balance beam and rotorod testing were analyzed by two-way ANOVA with repeated-measures performed to assess the effect of time and genotype, followed by Tukey's *post hoc* pairwise comparisons. For all other statistical analyses, comparisons were made using unpaired Student's *t*-test. Significance was established at $P < 0.05$.

For analysis of mitochondrial parameters in cultured motor neurons, one-way ANOVA followed by Tukey highly significant difference test was performed, with significance established at $P < 0.05$ (http://faculty.vassar.edu/lowry/VassarStats.html).

SUPPLEMENTARY MATERIAL

Supplementary Material is available at *HMG* online.

ACKNOWLEDGEMENTS

We thank the Fondation de l'Ataxie de Charlevoix-Saguenay for their constant support of this project. We also thank the Douglas Brain Bank of the Douglas Mental Health University Institute for providing us with the ARSACS brain tissues. We thank Joseph Rochford, PhD and Eve-Marie Charbonneau from the Neurophenotyping Centre at the Douglas Mental Health University Institute for conducting the behavioral study and for their technical expertise. We thank Robert Tanguay for his collaboration with the muscle histology.

Conflict of Interest statement. None declared.

FUNDING

This research was supported by Fondation de l'Ataxie de Charlevoix-Saguenay (www.arsacs.com) and the Canadian Institutes of Health Research Emerging team grant on rare diseases:Translating basic biology to enhanced patient care (126526).

REFERENCES

1. Bouchard, J.P., Barbeau, A., Bouchard, R. and Bouchard, R.W. (1978) Autosomal recessive spastic ataxia of Charlevoix-Saguenay. *Can. J. Neurol. Sci.*, **5**, 61–69.
2. Thiffault, I., Dicaire, M.J., Tetreault, M., Huang, K.N., Demers-Lamarche, J., Bernard, G., Duquette, A., Lariviere, R., Gehring, K., Montpetit, A. *et al.* (2013) Diversity of ARSACS mutations in French-Canadians. *Can. J. Neurol. Sci.*, **40**, 61–66.
3. Vingolo, E.M., Di Fabio, R., Salvatore, S., Grieco, G., Bertini, E., Leuzzi, V., Nesti, C., Filla, A., Tessa, A., Pierelli, F. *et al.* (2011) Myelinated retinal fibers in autosomal recessive spastic ataxia of Charlevoix-Saguenay. *Eur. J. Neurol.*, **18**, 1187–1190.
4. Garcia-Martin, E., Pablo, L.E., Gazulla, J., Polo, V., Ferreras, A. and Larrosa, J.M. (2013) Retinal nerve fibre layer thickness in ARSACS: myelination or hypertrophy? *Br. J. Ophthalmol.*, **97**, 238–241.
5. Bouchard, J.P., Barbeau, A., Bouchard, R. and Bouchard, R.W. (1998) Autosomal recessive spastic ataxia of Charlevoix-Saguenay. *Can. J. Neurol. Sci.*, **5**, 61–69.
6. Bouchard, J., Richter, A., Melancon, S., Mathieu, J. and Michaud, J. (2000) In Klockgether, K. (ed.), *Handbook of Ataxia Disorders*. Marcel Dekker, New York. pp. 311–324, Chapter 15: Autosomal recessive spastic ataxia (Charlevoix-Saguenay).
7. Bouchard, J. (1991) In JMBV, D.J. (ed.), *Handbook of Clinical Neurology. Hereditary Neuropathies and Spinocerebellar Atrophies*. Elsevier Science, New York City, Vol. 16, pp. 452–559.
8. Martin, M.H., Bouchard, J.P., Sylvain, M., St-Onge, O. and Truchon, S. (2007) Autosomal recessive spastic ataxia of Charlevoix-Saguenay: a report of MR imaging in 5 patients. Am. J. Neuroradiol., **28**, 1606–1608.
9. Baets, J., Deconinck, T., Smets, K., Goossens, D., Van den Bergh, P., Dahan, K., Schmedding, E., Santens, P., Rasic, V.M., Van Damme, P. *et al.* (2010) Mutations in SACS cause atypical and late-onset forms of ARSACS. *Neurology*, **75**, 1181–1188.
10. Duquette, A., Brais, B., Bouchard, J.P. and Mathieu, J. (2013) Clinical presentation and early evolution of spastic ataxia of Charlevoix-Saguenay. *Mov. Disord.*, **28**, 2011–2014.
11. Parfitt, D.A., Michael, G.J., Vermeulen, E.G., Prodromou, N.V., Webb, T.R., Gallo, J.M., Cheetham, M.E., Nicoll, W.S., Blatch, G.L. and Chapple, J.P. (2009) The ataxia protein sacsin is a functional co-chaperone that protects against polyglutamine-expanded ataxin-1. *Hum. Mol. Genet.*, **18**, 1556–1565.
12. Anderson, J.F., Siller, E. and Barral, J.M. (2010) The sacsin repeating region (SRR): a novel Hsp90-related supra-domain associated with neurodegeneration. *J. Mol. Biol.*, **400**, 665–674.
13. Anderson, J.F., Siller, E. and Barral, J.M. (2011) The neurodegenerative-disease-related protein sacsin is a molecular chaperone. *J. Mol. Biol.*, **411**, 870–880.
14. Greer, P.L., Hanayama, R., Bloodgood, B.L., Mardinly, A.R., Lipton, D.M., Flavell, S.W., Kim, T.K., Griffith, E.C., Waldon, Z., Maehr, R. *et al.* (2010) The Angelman syndrome protein Ube3A regulates synapse development by ubiquitinating arc. *Cell*, **140**, 704–716.
15. Kozlov, G., Denisov, A.Y., Girard, M., Dicaire, M.J., Hamlin, J., McPherson, P.S., Brais, B. and Gehring, K. (2011) Structural basis of defects in the sacsin HEPN domain responsible for autosomal recessive spastic ataxia of Charlevoix-Saguenay (ARSACS). *J. Biol. Chem.*, **286**, 20407–20412.
16. Girard, M., Lariviere, R., Parfitt, D.A., Deane, E.C., Gaudet, R., Nossova, N., Blondeau, F., Prenosil, G., Vermeulen, E.G., Duchen, M.R. *et al.* (2012) Mitochondrial dysfunction and Purkinje cell loss in autosomal recessive spastic ataxia of Charlevoix-Saguenay (ARSACS). *Proc. Natl. Acad. Sci. USA*, **109**, 1661–1666.
17. Louis, E.D., Faust, P.L., Vonsattel, J.P., Honig, L.S., Rajput, A., Rajput, A., Pahwa, R., Lyons, K.E., Ross, W.G., Elble, R.J. *et al.* (2009) Torpedoes in Parkinson's disease, Alzheimer's disease, essential tremor, and control brains. *Mov. Disord.*, **24**, 1600–1605.
18. Takahashi, N., Iwatsubo, T., Nakano, I. and Machinami, R. (1992) Focal appearance of cerebellar torpedoes associated with discrete lesions in the cerebellar white matter. *Acta Neuropathol.*, **84**, 153–156.
19. Yaginuma, M., Ishida, K., Uchihara, T., Suzuki, F., Aoki, M., Tanaka, T., Murase, H., Ikeda, K. and Mizusawa, H. (2000) Paraneoplastic cerebellar ataxia with mild cerebello-olivary degeneration and an anti-neuronal antibody: a clinicopathological study. *Neuropathol. Appl. Neurobiol.*, **26**, 568–571.

20. Smith, W.W., Liu, Z., Liang, Y., Masuda, N., Swing, D.A., Jenkins, N.A., Copeland, N.G., Troncoso, J.C., Pletnikov, M., Dawson, T.M. *et al.* (2010) Synphilin-1 attenuates neuronal degeneration in the A53T alpha-synuclein transgenic mouse model. *Hum. Mol. Genet.*, **19**, 2087–2098.
21. Vig, P.J., Shao, Q., Subramony, S.H., Lopez, M.E. and Safaya, E. (2009) Bergmann glial S100B activates myo-inositol monophosphatase 1 and Co-localizes to purkinje cell vacuoles in SCA1 transgenic mice. *Cerebellum*, **8**, 231–244.
22. Perrot, R., Berges, R., Bocquet, A. and Eyer, J. (2008) Review of the multiple aspects of neurofilament functions, and their possible contribution to neurodegeneration. *Mol. Neurobiol.*, **38**, 27–65.
23. Al-Chalabi, A. and Miller, C.C. (2003) Neurofilaments and neurological disease. *Bioessays*, **25**, 346–355.
24. Gentil, B.J., Minotti, S., Beange, M., Baloh, R.H., Julien, J.P. and Durham, H.D. (2012) Normal role of the low-molecular-weight neurofilament protein in mitochondrial dynamics and disruption in Charcot-Marie-Tooth disease. *FASEB J.*, **26**, 1194–1203.
25. Herrero, M.T., Barcia, C. and Navarro, J.M. (2002) Functional anatomy of thalamus and basal ganglia. Child*s Nerv. Syst.*, **18**, 386–404.
26. Schmahmann, J.D. (2003) Vascular syndromes of the thalamus. *Stroke*, **34**, 2264–2278.
27. Melo, T.P., Bogousslavsky, J., Moulin, T., Nader, J. and Regli, F. (1992) Thalamic ataxia. *J. Neurol.*, **239**, 331–337.
28. Prodi, E., Grisoli, M., Panzeri, M., Minati, L., Fattori, F., Erbetta, A., Uziel, G., D'Arrigo, S., Tessa, A., Ciano, C. *et al.* (2013) Supratentorial and pontine MRI abnormalities characterize recessive spastic ataxia of Charlevoix-Saguenay. A comprehensive study of an Italian series. *Eur. J. Neurol.*, **20**, 138–146.
29. Oguz, K.K., Haliloglu, G., Temucin, C., Gocmen, R., Has, A.C., Doerschner, K., Dolgun, A. and Alikasifoglu, M. (2013) Assessment of whole-brain white matter by DTI in autosomal recessive spastic ataxia of Charlevoix-Saguenay. Am. J. Neuroradiol., **34**, 1952–1957.
30. Singh, P., Yan, J., Hull, R., Read, S., O'Sullivan, J., Henderson, R.D., Rose, S., Greer, J.M. and McCombe, P.A. (2011) Levels of phosphorylated axonal neurofilament subunit H (pNfH) are increased in acute ischemic stroke. *J. Neurol. Sci.*, **304**, 117–121.
31. Anderson, K.J., Scheff, S.W., Miller, K.M., Roberts, K.N., Gilmer, L.K., Yang, C. and Shaw, G. (2008) The phosphorylated axonal form of the neurofilament subunit NF-H (pNF-H) as a blood biomarker of traumatic brain injury. *J. Neurotrauma*, **25**, 1079–1085.
32. Petzold, A. (2005) Neurofilament phosphoforms: surrogate markers for axonal injury, degeneration and loss. *J. Neurol. Sci.*, **233**, 183–198.
33. Perrot, R. and Eyer, J. (2009) Neuronal intermediate filaments and neurodegenerative disorders. *Brain Res. Bull.*, **80**, 282–295.
34. Forno, L.S., Sternberger, L.A., Sternberger, N.H., Strefling, A.M., Swanson, K. and Eng, L.F. (1986) Reaction of Lewy bodies with antibodies to phosphorylated and non-phosphorylated neurofilaments. *Neurosci. Lett.*, **64**, 253–258.
35. Lim, J., Hao, T., Shaw, C., Patel, A.J., Szabo, G., Rual, J.F., Fisk, C.J., Li, N., Smolyar, A., Hill, D.E. *et al.* (2006) A protein-protein interaction network for human inherited ataxias and disorders of Purkinje cell degeneration. *Cell*, **125**, 801–814.
36. Otey, C.A. and Carpen, O. (2004) Alpha-actinin revisited: a fresh look at an old player. *Cell. Motil. Cytoskeleton*, **58**, 104–111.
37. Wachsstock, D.H., Schwartz, W.H. and Pollard, T.D. (1993) Affinity of alpha-actinin for actin determines the structure and mechanical properties of actin filament gels. *Biophys. J.*, **65**, 205–214.
38. Pelletier, O., Pokidysheva, E., Hirst, L.S., Bouxsein, N., Li, Y. and Safinya, C.R. (2003) Structure of actin cross-linked with alpha-actinin: a network of bundles. *Phys. Rev. Lett.*, **91**, 148102.
39. Fuchs, E. and Cleveland, D.W. (1998) A structural scaffolding of intermediate filaments in health and disease. *Science (New York, NY)*, **279**, 514–519.
40. Leung, C.L., Sun, D., Zheng, M., Knowles, D.R. and Liem, R.K. (1999) Microtubule actin cross-linking factor (MACF): a hybrid of dystonin and dystrophin that can interact with the actin and microtubule cytoskeletons. *J. Cell Biol.*, **147**, 1275–1286.
41. Leung, C.L., Sun, D. and Liem, R.K. (1999) The intermediate filament protein peripherin is the specific interaction partner of mouse BPAG1-n (dystonin) in neurons. *J. Cell Biol.*, **144**, 435–446.
42. Rao, M.V., Mohan, P.S., Kumar, A., Yuan, A., Montagna, L., Campbell, J., Veeranna, Espreafico, E.M., Julien, J.P. and Nixon, R.A. (2011) The myosin Va head domain binds to the neurofilament-L rod and modulates endoplasmic reticulum (ER) content and distribution within axons. *PLoS ONE*, **6**, e17087.
43. Wagner, O.I., Lifshitz, J., Janmey, P.A., Linden, M., McIntosh, T.K. and Leterrier, J.F. (2003) Mechanisms of mitochondria-neurofilament interactions. *J. Neurosci.*, **23**, 9046–9058.
44. Luong, T.N., Carlisle, H.J., Southwell, A. and Patterson, P.H. (2011) Assessment of motor balance and coordination in mice using the balance beam. *J. Vis. Exp.*, **49**, 2376.
45. Durham, H.D., Roy, J., Dong, L. and Figlewicz, D.A. (1997) Aggregation of mutant Cu/Zn superoxide dismutase proteins in a culture model of ALS. *J. Neuropathol. Exp. Neurol.*, **56**, 523–530.
46. Roy, J., Minotti, S., Dong, L., Figlewicz, D.A. and Durham, H.D. (1998) Glutamate potentiates the toxicity of mutant Cu/Zn-superoxide dismutase in motor neurons by postsynaptic calcium-dependent mechanisms. *J. Neurosci.*, **18**, 9673–9684.